

Optimal Low Temperature Charging of Lithium-ion Batteries

Bharatkumar Suthar,* Dayaram Sonawane,** Richard D. Braatz,***
 Venkat R. Subramanian****^z

* Department of Energy, Environmental & Chemical Engineering, Washington University, St. Louis, MO, 63130

** Department of Chemical Engineering, University of Washington, Seattle, WA 98195, (e-mail: vsubram@uw.edu)

*** Department of Chemical Engineering, Massachusetts Institute of Technology, Cambridge, MA 02139

^zEnergy Processes and Materials Division, Pacific Northwest National Laboratory, Richland, WA 99354

Abstract: A lithium-plating side reaction at the lithiated graphite (LiC_6) anode leads to poor safety of the lithium-ion battery. Faster charging at normal temperature may lead to a plating side reaction during the end of charging at the anode-separator interface. At lower temperature, the lithium-plating side reaction may become thermodynamically favorable during almost the entire charging period, even at low rates. This paper uses an electrochemical engineering model and dynamic optimization framework to derive charging profiles to minimize lithium plating at low temperatures. Transport parameters for lithium-ion battery are very sensitive at low temperatures. This paper shows the derivation of the optimal charging profile considering strict lower bounds on the plating reaction depending on various thermal insulation conditions (adiabatic, isothermal, and normal heat transfer coefficient) surrounding the battery.

© 2015, IFAC (International Federation of Automatic Control) Hosting by Elsevier Ltd. All rights reserved.

Keywords: Li-ion battery, dynamic optimization, plating reaction, optimal charging, capacity fade.

1. INTRODUCTION

Lithium-ion chemistries are attractive for many applications due to high cell voltage, high volumetric and gravimetric energy density (100 Wh/kg), high power density (300 W/kg), good temperature range, low memory effect, and relatively long battery life (Daniel, 2008; Lukic et al., 2008; Pop et al., 2008). Capacity fade, underutilization, and thermal runaway are the main issues that need to be addressed in order to use a lithium-ion battery efficiently and safely over a long life.

The focus of this work is to address the lithium-plating side reaction, which not only causes capacity fade but also poses a significant safety issue (Tarascon and Armand, 2001). Though lithium-ion batteries are inherently safer than lithium-metal batteries, because the former avoids dendrite formation during charging, the slightly more positive potential of LiC_6 compared to Li/Li^+ inherits the problem of lithium plating during charging (Tarascon and Armand, 2001) at high rates (Northrop et al., 2014) and even for low rates at low temperature.

The driving force for the irreversible lithium-plating side reaction at the anode can be expressed by the over-potential (Perkins et al., 2012):

$$\eta_{\text{plating}} = \phi_n^s(x, t) - \phi_{e,n}(x, t) - U_s \quad (1)$$

where η_{plating} is the plating over-potential, $\phi_n^s(x, t)$ is the solid-phase potential which is defined for the porous electrode, $\phi_{e,n}(x, t)$ is the electrolyte-phase potential, U_s is the open-circuit potential for the plating reaction which is taken to be zero, and x is the distance across the electrode. The expression for η_{plating} in (1) ignores the voltage drop

across the solid-electrolyte interface (SEI) layer. The lithium-plating side reaction becomes feasible only when η_{plating} is negative as the plating reaction is irreversible in nature. Detailed electrochemical engineering-based models incorporating concentrated solution theory and porous electrode theory that can simulate the potential distribution inside porous structures are available (Arora et al., 1999; Doyle et al., 1993; Doyle and Newman, 1995; Fuller et al., 1994; Gomadam et al., 2002).

In this paper, a single-particle model (Guo et al., 2011; Santhanagopalan et al., 2006) (SPM) is used to derive the optimal charging profiles. The SPM ignores the distribution of concentration and potential across the thicknesses of the electrodes and separator. At low temperature, η_{plating} (the x dependency does not appear in the SPM) shifts down due to increased temperature-dependent transport resistance and may become negative even for the beginning of charging, which makes the battery vulnerable to lithium plating even at low charging rate for these temperatures.

Section 2 discusses the SPM along with its equations and presents simulation results for charging a battery at low temperature (268 K). Section 3 discusses the optimal charging problem formulation. The results and discussion are in Section 4 and the conclusions and future directions are in Section 5.

2. MODEL DESCRIPTION

Detailed models that incorporate electrochemical, transport, and thermodynamic processes along with the geometry of the underlying system can be used to monitor and control the internal states of a battery (Arora et al., 1999; Doyle et al., 1993; Doyle and Newman, 1995; Fuller et al., 1994;

Gomadani et al., 2002). Simplifications of these models have been proposed that preserve the important features of detailed models. The SPM assumes that the porous nature of the solid phase in the anode and cathode can be approximated by the dynamics of a single particle. The SPM also ignores the dynamics and variation of lithium-ion concentration in the electrolyte phase.

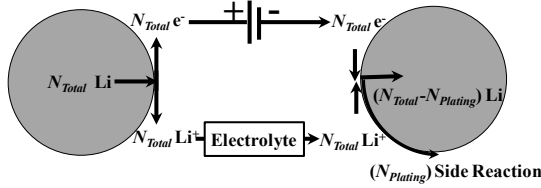


Fig. 1. Conceptual diagram of the plating side reaction.

Figure 1 is a conceptual diagram of the plating side reaction in the SPM framework. Table 1 shows the governing equations for the SPM (Guo et al., 2011; Santhanagopalan et al., 2006), which models Fickian diffusion in the solid particle, where $c_i^s(r, t)$ is the solid-phase lithium concentration ($i = n$ and p for anode and cathode respectively) which has radial and time dependence, V is the voltage across the battery, T is the temperature of the battery, and ϕ_i^s refers to the potential of the solid particles. The equation for the temperature is derived from the general energy balance. A simplified energy balance equation ignoring the reversible heat caused by the reaction entropy change is used in this study. These simplifications may lead to less accurate prediction of the variables at the cell level. The solid-phase diffusivities (D_i) of both anode and cathode particles are assumed to follow an Arrhenius-type relationship, as shown in Table 2, which also shows the additional expressions used in the SPM. A list of parameters and their values are in Appendices A and B.

Table 1: Governing equations for the single-particle model

Positive Electrode: Solid-phase concentration $c_p^s(r, t)$		
Governing equation	Boundary conditions	
$\frac{\partial c_p^s}{\partial t} = \frac{1}{r^2} \frac{\partial}{\partial r} \left[r^2 D_p^s \frac{\partial c_p^s}{\partial r} \right]$	$\frac{\partial c_p^s}{\partial r} \Big _{r=0} = 0, -D_p^s \frac{\partial c_p^s}{\partial r} \Big _{r_p} = \frac{I_{\text{overall}}}{a_p F}$	(2)
Negative Electrode: Solid-phase concentration $c_n^s(r, t)$		
Governing equations	Boundary conditions	
$\frac{\partial c_n^s}{\partial t} = \frac{1}{r^2} \frac{\partial}{\partial r} \left[r^2 D_n^s \frac{\partial c_n^s}{\partial r} \right]$	$\frac{\partial c_n^s}{\partial r} \Big _{r=0} = 0, -D_n^s \frac{\partial c_n^s}{\partial r} \Big _{r_n} = \frac{-I_{\text{overall}}}{a_n F}$	(3)
Voltage: $V(t) = \phi_p^s(t) - \phi_n^s(t) + I_{\text{overall}} R_{\text{cell}}$		(4)
Temperature: $T(t)$		
$m C_p \frac{dT(t)}{dt} = I_{\text{overall}} (\eta_p - \eta_n + I_{\text{overall}} R_{\text{cell}}) - h A_{HT} (T(t) - T_{\text{amb}})$		(5)

Table 2: Additional expressions used in the SPM

$\frac{I_{\text{overall}}}{a_p F} = k_p \sqrt{c_p^s c_{p,\text{surf}}^s (1 - c_{p,\text{surf}}^s)} \sinh \left(F (\phi_p^s - \phi_{e,p} - U_p) / (2RT) \right)$	(6)
$\frac{-I_{\text{overall}}}{a_n F} = k_n \sqrt{c_n^s c_{n,\text{surf}}^s (1 - c_{n,\text{surf}}^s)} \sinh \left(F (\phi_n^s - \phi_{e,n} - U_n) / (2RT) \right)$	(7)
$a_i = (3/R) (1 - \varepsilon_i - \varepsilon_{f,i}) A_{\text{cross}} l_i, i = p, n$	(8)
$U_p = \frac{\begin{pmatrix} -4.656 + 88.669 \theta_p^2 - 401.119 \theta_p^4 + \\ 342.909 \theta_p^6 - 462.471 \theta_p^8 + 433.434 \theta_p^{10} \\ -1.0 + 18.933 \theta_p^2 - 79.532 \theta_p^4 + 37.311 \theta_p^6 \\ -73.083 \theta_p^8 + 95.96 \theta_p^{10} \end{pmatrix}}{\theta_p = \frac{c^s _{r=R_p}}{c_{\text{max},p}^s}}$	(9)
$U_n = \frac{\begin{pmatrix} 0.7222 + 0.1387 \theta_n + 0.029 \theta_n^{0.5} - \\ 0.0172 \theta_n^{-1} + 0.0019 \theta_n^{-1.5} + \\ 0.2808 e^{0.9-15 \theta_n} - 0.7984 e^{0.4465 \theta_n - 0.4108} \end{pmatrix}}{\theta_n = \frac{c^s _{r=R_n}}{c_{\text{max},n}^s}}$	(10)
$D_i^s = D_{i,\text{ref}}^s \exp \left(- \left(E_a^{D_i^s} / R \right) [1/T - 1/T_{\text{ref}}] \right), i = p, n$	(11)
$k_i = k_{i,\text{ref}} \exp \left(- \left(E_a^{k_i} / R \right) [1/T - 1/T_{\text{ref}}] \right), i = p, n$	(12)

Before considering an optimal control formulation, it is useful to evaluate the potential for lithium plating at low temperatures. Three different cases (isothermal, $h = 25$ W/m²-K and adiabatic) are considered to understand the internal state evolution during charging at 268 K. Figure 2 shows the simulation results (current, voltage, plating over-potential, and temperature profiles) with the SPM at three different heat transfer coefficients for a 1.5 C rate of constant current charging followed by constant potential charging (CC-CV). This type of charging is considered the traditional charging protocol. The time evolution of plating over-potential at room temperature follows similar trends but the values remains around 0.03 to 0.1 V at 2C rate with a normal heat transfer coefficient (Northrop et al., 2014).

For the adiabatic case, the battery temperature increases faster leading to reduced transport resistance (diffusion and kinetic), which will lead to a lower observed voltage across the battery during charging. The battery in this case is less vulnerable to the plating side reaction with the plating side reaction being feasible ($\phi_n^s(t) - \phi_{e,n}(t) < 0$) only for small and intermediate times (see Figure 2, solid green curves). Isothermal charging (dashed black curves in Figure 2) is the worst-case scenario, with the plating reaction being feasible for a longer period of time. For a normal heat transfer coefficient (dotted red curves in Figure 2), the situation is in between the two cases (isothermal and adiabatic charging). In the next section, the optimal charging problem is formulated to obtain charging profiles that restrict the over-potential for plating at 0 V.

3. OPTIMAL CONTROL FORMULATION

This paper considers the maximization of charge transferred in a limited time with constraints placed on current, voltage, and plating over-potential using the SPM. Previous efforts in this direction include the derivation of optimal charging profiles considering other capacity fade mechanics (side reaction during charging (Rahimian et al., 2010), thermal

degradation (Suthar et al., 2013), and intercalation-induced stress using SPM (Suthar et al., 2014)). Numerous methods are available for solving constrained dynamic optimization problems, including (i) variational calculus, (ii) Pontryagin's maximum principle, (iii) control vector iteration, (iv) control vector parameterization, and (v) simultaneous nonlinear programming (e.g., Biegler, 2007; Kameswaran and Biegler, 2006; Canon et al., 1970). Control vector parameterization (CVP) and simultaneous nonlinear programming are commonly used strategies that employ nonlinear programming (NLP) solvers. This paper uses IPOPT, which implements an interior point primal-dual method (Wächter and Biegler, 2006).

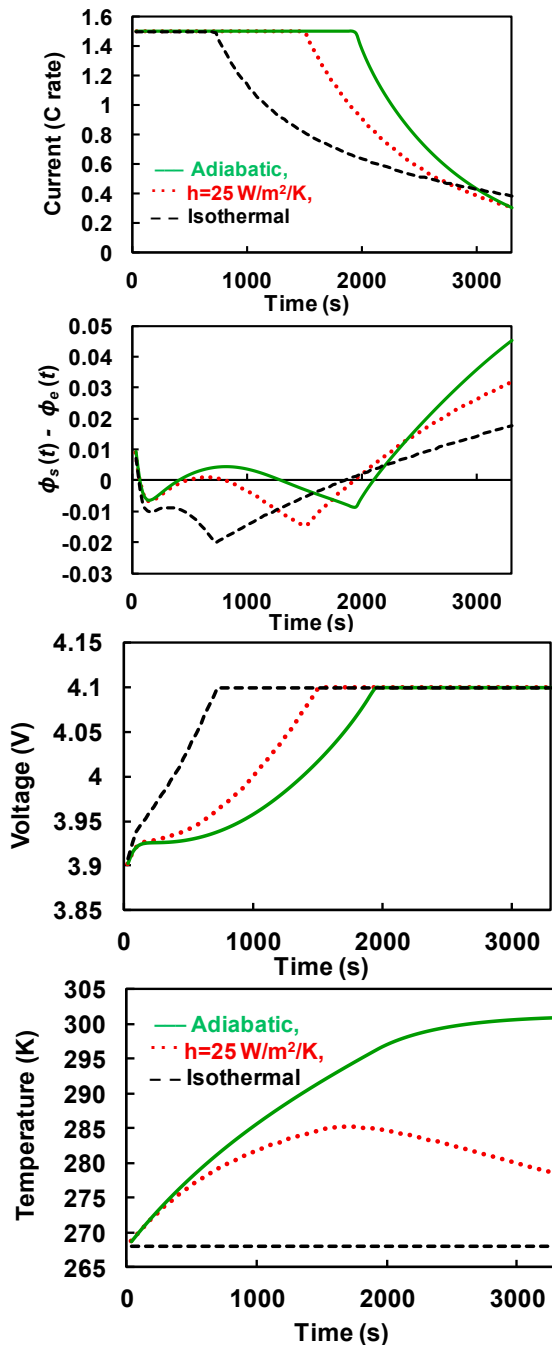


Fig. 2. SPM simulation at different heat transfer coefficients with CC-CV at 1.5 C at 268 K.

Consider the optimal charging profile with fixed final time (3300 s) and with the objective of maximizing stored charge. The optimal control problem of interest can be formulated as (in discretized version):

$$\begin{aligned} & \max_{I_{\text{overall}}(k)} \sum_{k=1}^N I_{\text{overall}}(k); \\ & \text{such that:} \\ & F_k(z(k+1), z(k), y(k), I_{\text{overall}}(k)) = 0 \\ & G_k(z(k), y(k), i_{\text{applied}}(k)) = 0 \\ & \text{initial conditions } z(k=1) = z_0 \text{ and bounds} \\ & 0 \leq I_{\text{overall}}(k) \leq I_{\text{max}}, \quad y_{\text{min}} \leq y(k) \leq y_{\text{max}}, \\ & z_{\text{min}} \leq z(k) \leq z_{\text{max}}, \end{aligned} \quad (13)$$

with F_k differential equation constraints, G_k algebraic equation constraints, N time discretizations, z differential states, y algebraic states, and an applied current of $I_{\text{overall}}(k)$. The differential state constraints include physically meaningful bounds on the solid-phase lithium concentration in the anode and cathode solid particle. Meaningful bounds are also provided for the algebraic states (e.g., $2.8 \leq V(k) \leq 4.1$, $0 \leq \eta_{\text{plating}}(k)$) and the control variable ($0 \leq I_{\text{overall}}(k) \leq I_{\text{max}}$).

4. RESULTS AND DISCUSSION

A fourth-order accurate finite difference method (third-order accurate at the boundaries) is used to discretize the diffusion equation in the solid particles in the radial direction to generate system of differential algebraic equations (DAEs). The discretized version of the partial differential equation (2) at the κ th internal node point in the radial direction in the solid particles of the anode and cathode (κ starts at 2) is

$$\frac{dc_{i,\kappa}^s(t)}{dt} = \frac{D_i^s}{(dr)^2} \left\{ \frac{(c_{i,\kappa-2}^s(t) - 8c_{i,\kappa-1}^s(t) + 8c_{i,\kappa+1}^s(t) - c_{i,\kappa+2}^s(t))}{6(\kappa-1)} + \frac{1}{12} \left(-c_{i,\kappa-2}^s(t) + 16c_{i,\kappa-1}^s(t) - 30c_{i,\kappa}^s(t) + 16c_{i,\kappa+1}^s(t) - c_{i,\kappa+2}^s(t) \right) \right\} \quad (14)$$

A similar discretization was performed to convert the PDE (3) to a set of ordinary differential equations (ODEs). These ODEs along with the equation for temperature (an ODE), voltage (an algebraic equation), and boundary conditions for the solid particles (algebraic equations) lead to a system of DAEs. The first-order Euler backward scheme was used to discretize the resulting system of DAEs into algebraic equations. The nonlinear program was solved using IPOPT (Wächter and Biegler, 2006).

Figure 3 shows the optimization results for I_{max} set to 1.5C. For isothermal charging (black dashed curves), the charging profile is mostly governed by the plating over-potential and overall voltage. During isothermal charging, the temperature-dependent transport parameters do not vary and the stored charge in a given time is lowest compared to the other cases where the transport resistance decreases.

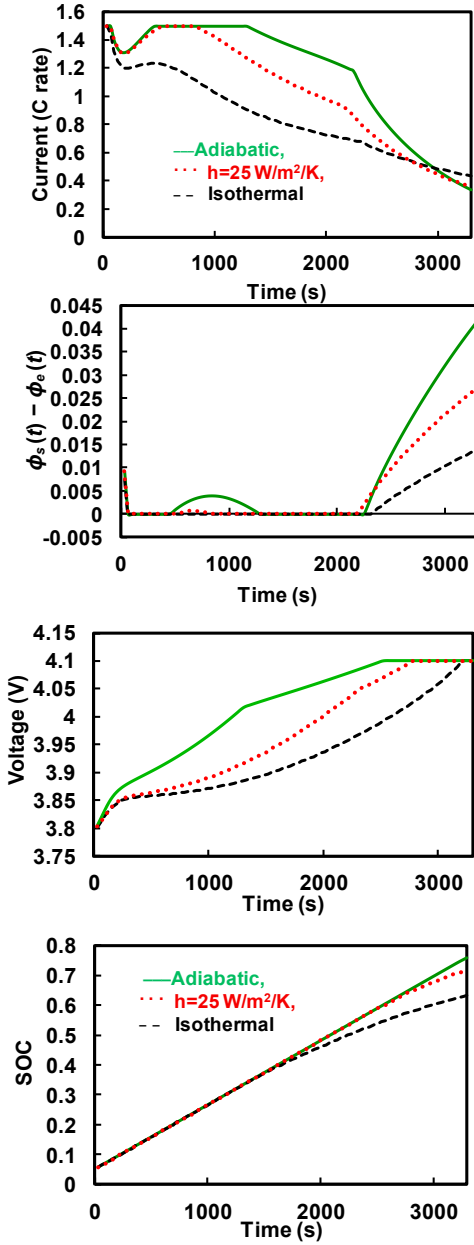


Fig. 3. Optimization results at 268 K at $I_{\max} = 1.5C$ with minimum bound on η_{plating} (SOC refers to state of charge).

Charging in the adiabatic and normal cases (heat transfer coefficient = $25 \text{ W/m}^2\text{K}$) show very interesting profiles. In both cases, the charging profiles are controlled by different active constraints at different times. The optimal charging current consists of five segments, each being governed/controlled by an active constraint. Initially, the maximum charging current (I_{\max}) acts as the active constraints for a very small time followed by the plating over-potential (η_{plating}) constraint. Later, the dynamics of $\phi_n(t) - \phi_e(t)$ play a significant role in determining the shape of the optimal charging profile. As η_{plating} recovers ($\phi_n(t) - \phi_e(t) > 0$), the current takes the maximum value followed by η_{plating} becoming the active constraint. The end of charging is then controlled by the voltage drop (V) across of the battery.

The optimal charging profiles for different values of I_{\max} can be generated in a similar fashion. As can be seen from Figure 4 for $I_{\max} = 1C$, the charge stored or state of charge (SOC) in adiabatic charging is significantly higher compared to other cases. In the case of adiabatic charging, $\phi_n(t) - \phi_e(t)$ remains positive throughout charging, hence η_{plating} never becomes an active constraint, which gives rise to the traditional CC-CV charging profile (green solid curves in Figure 4). For a normal heat transfer coefficient and isothermal charging, η_{plating} becomes the active path constraint during the charging process.

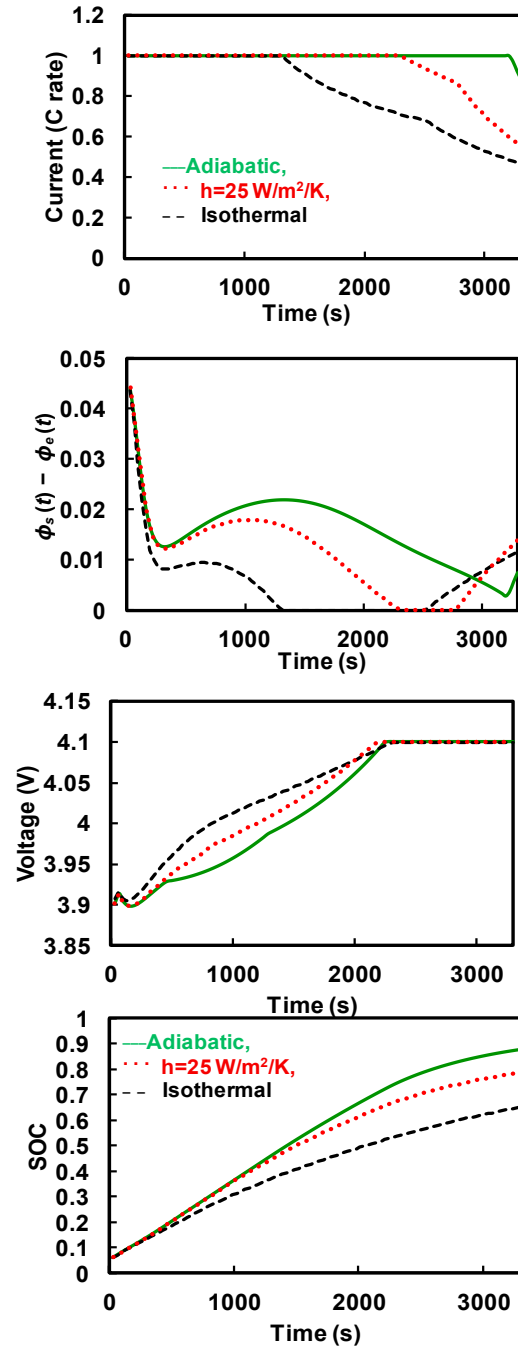


Fig. 4. Optimization results at 268 K at $I_{\max} = 1C$ with minimum bound on η_{plating} .

It is clear from the two cases that, at lower temperature, even the 1C rate of CC-CV charging is not the best charging protocol when η_{plating} is considered. The dynamics of η_{plating} dominates the charging profile and hence model-based optimal charging profiles are advised when charging batteries at lower temperatures. Use of electrochemical engineering model-based charging profiles requires robust estimation of transport parameters and their temperature dependence.

While most simulations were performed with Euler backward (EB) method, the result was verified by attempting few trial cases using the fifth-order Radau IIA (R-IIA) method (Kameswaran and Biegler, 2008). Table 3 shows solutions comparison between first-order EB and R-IIA for the isothermal charging case with $I_{\text{max}} = 1\text{C}$. From Table 3, it is observed that, although one-step EB method has a lower CPU time than that of R-IIA for a given number of node points, R-IIA can achieve higher order of accuracy even at lower node points. However, R-IIA has 3 times the number of variables compared to EB method for same number of node points. In many cases, faster results can be obtained with R-IIA or other types of higher order discretization schemes.

Table 3: Solution time comparison for $I_{\text{max}} = 1\text{C}$ (isothermal)

Node Points	Objective Value		CPU Time (s)	
	EB	Radau-IIA	EB	Radau-IIA
10	0.6267167	0.6343626	0.224	0.697
20	0.6303987	0.6343439	0.417	1.748
50	0.6327567		0.615	
100	0.6335656		0.967	
200	0.6342731		2.085	

These optimization studies performed using the SPM may not be very accurate at lower temperature. Use of a porous pseudo-two dimensional (P2D) model will be pursued for identifying the charging protocol because of the expected non-uniform current density.

4. CONCLUSIONS

This paper addresses lithium plating during charging at low temperature, which is closely related to the safe operation of a lithium-ion battery. A single-particle model, which makes significant simplification in transport processes, is used with a general energy balance equation with additional simplification. Although this model has some limits on its applicability for prediction of the internal variables when used at the cell level, the optimal control problem formulated here places a lower bound on η_{plating} in addition to voltage and current bounds. The dynamic optimization framework is used to quickly predict the optimal charging profiles for different environmental conditions and bounds. Accurate prediction as well as a P2D model for modeling spatial variation of η_{plating} can be used to further refine the charging protocol, which will be performed in the future. The proposed framework offers an alternative of calculating real-time optimal charging profiles, provided that temperature-dependent transport parameters are known.

ACKNOWLEDGMENTS

The authors are thankful for the financial support from the United States Government, Advanced Research Projects Agency – Energy (ARPA-E), U.S. Department of Energy, under award number DE-AR0000275, and the McDonnell International Scholar Academy at Washington University in St. Louis.

REFERENCES

- Arora, P., Doyle, M., & White, R. E. (1999). Mathematical modeling of the lithium deposition overcharge reaction in lithium-ion batteries using carbon-based negative electrodes. *Journal of the Electrochemical Society*, 146, 3543-3553.
- Biegler, L. T. (2007). An overview of simultaneous strategies for dynamic optimization. *Chemical Engineering and Processing: Process Intensification*, 46, 1043-1053.
- Canon, M. D., Cullum, C. D., Jr., & Polak, E. (1970). *Theory of Optimal Control and Mathematical Programming*, New York, McGraw-Hill.
- Daniel, C. (2008). Materials and processing for lithium-ion batteries. *JOM*, 60, 43-48.
- Doyle, M., Fuller, T. F., & Newman, J. (1993). Modeling of Galvanostatic Charge and Discharge of the Lithium Polymer Insertion Cell. *Journal of the Electrochemical Society*, 140, 1526-1533.
- Doyle, M. & Newman, J. (1995). The use of mathematical modeling in the design of lithium/polymer battery systems. *Electrochimica Acta*, 40, 2191-2196.
- Fuller, T. F., Doyle, M. & Newman, J. (1994). Simulation and optimization of the dual lithium ion insertion cell. *Journal of the Electrochemical Society*, 141, 1.
- Gomadam, P. M., Weidner, J. W., Dougal, R. A., & White, R. E. (2002). Mathematical modeling of lithium-ion and nickel battery systems. *Journal of Power Sources*, 110, 267-284.
- Guo, M., Sikha, G. & White, R. E. (2011). Single-particle model for a lithium-ion cell: thermal behavior. *Journal of the Electrochemical Society*, 158, A122-A132.
- Kameswaran, S. & Biegler, L. (2008). Convergence rates for direct transcription of optimal control problems using collocation at Radau points. *Computational Optimization and Applications*, 41, 81-126.
- Kameswaran, S. & Biegler, L. T. (2006). Simultaneous dynamic optimization strategies: Recent advances and challenges. *Computers & Chemical Engineering*, 30, 1560-1575.
- Lukic, S. M., Cao, J., Bansal, R. C., Rodriguez, F. & Emadi, A. (2008). Energy storage systems for automotive applications. *IEEE Transactions on Industrial Electronics*, 55, 2258-2267.
- Northrop, P. W. C., Suthar, B., Ramadesigan, V., Santhanagopalan, S., Braatz, R. D., & Subramanian, V. R. (2014). Efficient simulation and reformulation of lithium-ion battery models for enabling electric transportation. *Journal of the Electrochemical Society*, 161, E3149-E3157.
- Perkins, R. D., Randall, A. V., Zhang, X., & Plett, G. L. (2012). Controls oriented reduced order modeling of

- lithium deposition on overcharge. *Journal of Power Sources*, 209, 318-325.
- Pop, V., Bergveld, H. J., Danilov, D., Regtien, P. P. L., & Notten, P. H. L. (2008). *Battery Management Systems: Accurate State-of-Charge Indication for Battery Powered Applications*, Dordrecht, Springer.
- Rahimian, S. K., Rayman, S. C., & White, R. E. (2010). Maximizing the life of a lithium-ion cell by optimization of charging rates. *Journal of the Electrochemical Society*, 157, A1302-A1308.
- Santhanagopalan, S., Guo, Q., Ramadass, P., & White, R. E. (2006). Review of models for predicting the cycling performance of lithium ion batteries. *Journal of Power Sources*, 156, 620-628.
- Subramanian, V. R., Boovaragavan, V., Ramadesigan, V., & Arabandi, M. (2009). Mathematical model reformulation for lithium-ion battery simulations: galvanostatic boundary conditions. *Journal of the Electrochemical Society*, 156, A260-A271.
- Suthar, B., Ramadesigan, V., De, S., Braatz, R. D., & Subramanian, V. R. (2014). Optimal charging profiles for mechanically constrained lithium-ion batteries. *Physical Chemistry Chemical Physics*, 16, 277-287.
- Suthar, B., Ramadesigan, V., Northrop, P. W. C., Gopaluni, B., Santhanagopalan, S., Braatz, R. D., & Subramanian, V. R. (2013). Optimal control and state estimation of lithium-ion batteries using reformulated models. *Proceedings of the American Control Conference*, 5350-5355.
- Tarascon, J.-M. & Armand, M. (2001). Issues and challenges facing rechargeable lithium batteries. *Nature*, 414, 359-367.
- Wächter, A. & Biegler, L. T. (2006). On the implementation of an interior-point filter line-search algorithm for large-scale nonlinear programming. *Mathematical Programming*, 106, 25-57.

Appendix A: LIST OF VARIABLES

a_i	Total surface area of electrode (m^2)
c_i^s	Solid-phase concentration
$c_{i,\max}^s$	Maximum solid-phase concentration
$c_{i,0}^s$	Initial solid-phase concentration
c_e	electrolyte concentration
C_p	Heat capacity
$D_{i,\text{ref}}^s$	Solid-phase diffusivity
$E_a^{D_i^s}$	Activation energy for diffusivities
$E_a^{k_i}$	Activation energy for the reaction rate
F	Faraday's constant
I_{overall}	Current (A)
$k_{i,\text{ref}}$	Reference reaction rate constant
k	Discretization index in time domain
κ	Discretization index in radial direction
l_i	Region thickness
m	Total mass of the battery

N	Time discretizations
N_{Total}	Total intercalated lithium
N_{Plating}	Lithium lost in the plating reaction
η	Over-potential
ϕ_i^s	Solid-phase potential
$\phi_{e,i}$	Electrolyte-phase potential
$R_{p,i}$	Particle radius
R	Gas constant
R_{cell}	Effective resistance of the electrolyte
R	Radial coordinate
$T_{\text{ref}}, T_{\text{amb}}$	Reference and ambient temperature
U	Open-circuit potential
$\varepsilon_{f,i}$	Filler fraction
ε_i	Porosity
A_{cross}	Cross-sectional area of the electrode
hA_{HT}	Heat transfer coefficient \times area

Subscripts:

e	Related to electrolyte
n	Related to the negative electrode—the anode
p	Related to the positive electrode—the cathode
Surf	Related to surface ($r = R_p$ or R_n)

Appendix B: LIST OF PARAMETERS AND VALUES

	Cathode ^a	Separator ^a	Anode ^a	Units
$\frac{a_i}{A_{\text{cross}} l_i}$	354000		144720	m^2/m^3
$c_{i,\max}^s$	51554		30555	mol/m^3
$c_{i,0}^s$	48976.3		3208.27	mol/m^3
c_e		1000		mol/m^3
C_p		823		$\text{J}/\text{kg}\cdot\text{K}$
$D_{i,\text{ref}}^s$	1×10^{-14}		3.9×10^{-14}	m^2/s
$E_a^{D_i^s}$	29000 ^b		35000 ^b	J/mol
$E_a^{k_i}$	58000 ^b		20000 ^b	J/mol
F		96487		C/mol
$k_{i,0}$	2.33×10^{-11}		5×10^{-10}	$\frac{\text{m}^{2.5}}{(\text{mol}^{0.5}\text{s})}$
l_i	80×10^{-6}	25×10^{-6}	88×10^{-6}	m
m		44×10^{-3}		kg
$R_{p,i}$	5×10^{-6} ^b		10×10^{-6} ^b	m
R		8.314		$\text{J}/\text{mol}\cdot\text{K}$
T_{ref}		298.15		K
$\varepsilon_{f,i}$	0.025		0.0326	
ε_i	0.385	0.724	0.485	
hA_{HT}		0.02		W/K

^a Unless otherwise noted, all parameters used for the electrodes and separator are from Subramanian et al. (2009)

^b Assumed value